Single-Crystal Growth of Ln_2MIn_8 (Ln = La, Ce; M = Rh, Ir): Implications for the Heavy-Fermion Ground State

Robin T. Macaluso,[†] J. L. Sarrao,[‡] N. O. Moreno,[‡] P. G. Pagliuso,[‡] J. D. Thompson,[‡] Frank R. Fronczek,[†] M. F. Hundley,[‡] A. Malinowski,[‡] and Julia Y. Chan*[,†]

Department of Chemistry, Louisiana State University, Baton Rouge, Louisiana 70803, and Los Alamos National Laboratory, Los Alamos, New Mexico 87545

Received October 28, 2002. Revised Manuscript Received January 16, 2003

The structures of the heavy-fermion compounds, Ce_2MIn_8 (M = Rh, Ir), and the nonmagnetic analogues, La_2MIn_8 (M = Rh, Ir), were determined by single-crystal X-ray diffraction. These materials adopt a tetragonal structure in the space group $P4/mmm$, $Z = 1$. Lattice parameters are $a = 4.6670(4)$ Å and $c = 12.247(4)$ Å for Ce_2RhIn_8, $a = 4.6897(6)$ Å and $c = 12.1950(11)$ Å for Ce_2IrIn_8, $a = 4.6980(2)$ Å and $c = 12.3440(4)$ Å for La_2RhIn_8, and $a = 4.70600(10)$ Å and $c = 12.3120(4)$ Å for La_2IrIn_8. Antiferromagnetism and/or unconventional superconductivity at low temperature have been found in $CeCoIn_5$, $CeRhIn_5$, $CeIrIn_5$, and Ce_2RhIn_8. We compare structural trends with properties of the ground states of these materials. The Ln_nMIn_{3n+2} ($n = 1, 2, \infty$; Ln = La, Ce; M = Rh, Ir) intergrowth homologous series presents a unique opportunity to study structure−property relationships in this new family of heavy-fermions.

Introduction

Superconductivity in heavy-fermion materials is unconventional because the conduction electrons are strongly coupled with the magnetic moments of the *f*-electrons.[1] At room temperature, heavy-fermion materials behave as normal metals in which the *f*-electrons interact weakly with conduction electrons and display local-moment magnetic properties, but at low temperatures ($T \leq 20$ K), unique and interesting properties appear. The strong hybridization between conduction electrons and *f*-electrons results in an enhanced linear-in-temperature contribution to the Sommerfeld coefficient of specific heat, γ, (with γ typically ≥ 400 mJ/mol K^2). This corresponds to the conduction electrons having an effective mass that is typically 100 times that of a free electron, hence the term, "heavy-fermion."[2] The hybridization that produces heavy-fermion properties derives from the local coordination of the *f*-electron ion.

The properties of the new intergrowth homologous series, Ce_nMIn_{3n+2} ($n = 1, 2$; M = Co, Rh, Ir) have been recently reported and present a unique opportunity to investigate the structure−property relationships of these heavy-fermion superconductors.[3−5] $CeCoIn_5$ and $CeIrIn_5$ are superconducting at 2.3 and 0.4 K, respectively, while $CeRhIn_5$ superconducts at 2.1 K under applied pressures of 16 kbar.[4,5] At ambient pressure, $CeRhIn_5$ is a heavy-fermion antiferromagnet with an incommensurate magnetic structure and $T_N = 3.8$ K.[3,6,7]

Similar to $CeRhIn_5$, Ce_2RhIn_8 orders antiferromagnetically at $T_N = 2.8$ K at ambient pressure, but superconductivity with $T_c \sim 2$ K can be induced with the application of ~25 kbar of pressure.[8] The Sommerfeld constant $\gamma \approx 400$ mJ/mole K^2 of Ce_2RhIn_8 is also comparable to that of $CeRhIn_5$. The fact that the superconducting transition temperature is higher in $CeRhIn_5$ and Ce_2RhIn_8 than in $CeIn_3$ and the nature of magnetic structure in these materials have been attributed to their quasi-layered structure relative to $CeIn_3$.

Ce_2IrIn_8, on the other hand, remains paramagnetic to lowest temperatures. Although it has a Sommerfeld coefficient similar to that of $CeIrIn_5$ ($\gamma \approx 700$ mJ/mol K^2), it does not display superconductivity. Although it is not the subject of this paper and its ground-state properties are unknown, polycrystalline Ce_2CoIn_8 has been synthesized and found to be isostructural to the Rh and Ir compounds.

$CeIn_3$ (the "parent" and $n = \infty$ member of Ce_nMIn_{3n+2}) is cubic and undergoes a commensurate antiferromagnetic transition at $T_N = 10.23$ K.[9,10] It also becomes

* Corresponding author e-mail: julia.chan@chem.lsu.edu.
[†] Louisiana State University.
[‡] Los Alamos National Laboratory.

(1) Fisk, Z.; Ott, H. R.; Rice, T. M.; Smith, J. L. *Science* **1986**, *320*, 124.
(2) Cornelius, A. L.; Pagliuso, P. G.; Hundley, M. F.; Sarrao, J. L. *Phys. Rev. B* **2002**, *64*, 144411.
(3) Hegger, H.; Moshopoulou, E. G.; Hundley, M. F.; Sarrao, J. L.; Fisk, Z.; Thompson, J. D. *Phys. Rev. Lett.* **2000**, *84*, 4986.
(4) Petrovic, C.; Pagliuso, P. G.; Hundley, M. F.; Movshovich, R.; Sarrao, J. L.; Thompson, J. D.; Fisk, Z.; Monthoux, P. *J. Phys.: Condens. Matter* **2001**, *13*, L337.
(5) Petrovic, C.; Movshovich, R.; Jaime, M.; Pagliuso, P. G.; Hundley, M. F.; Sarrao, J. L.; Fisk, Z.; Thompson, J. D. *Europhys. Lett.* **2001**, *53*, 354.
(6) Bao, W.; Aeppli, G.; Christianson, A. D.; Fisk, Z.; Hundley, M. F.; Lacerda, A. H.; Lynn, J. W.; Pagliuso, P. G.; Sarrao, J. L.; Thompson, J. D. *World Scientific* **2002**, In press.
(7) Bao, W.; Pagliuso, P. G.; Sarrao, J. L.; Thompson, J. D.; Fisk, Z.; Lynn, J. W. *Phys. Rev. B* **2002**, *64*, 020401(R).
(8) Nicklas, M.; Sidorov, V. A.; Borges, H. A.; Pagliuso, P. G.; Petrovic, C.; Fisk, Z.; Sarrao, J. L.; Thompson, J. D. http://xxx.lanl.gov 2002, arXiv:cond.

10.1021/cm021063e CCC: $25.00
Published on Web 03/04/2003

superconducting between 24 and 27.5 kbar pressure with the sharpest transition at $T_c = 0.204$ K and 27.5 kbar.[11,12] The low-temperature linear contribution to specific heat of $CeIn_3$ is $\gamma \approx 120$ mJ/mol K^2.[13−15]

The principal focus of this work is the growth and structural characterization of the $n = 2$ members of the Ce_nMIn_{3n+2}. The La analogues of these Ce compounds have also been prepared with the aim of understanding which structural trends derive specifically from the presence of an *f*-electron in the Ce compounds. In this study, the structure and magnetic properties of the $n = 1, 2, \infty$ members of the intergrowth homologous series of compounds, Ln_nMIn_{3n+2} (Ln = La, Ce; M = Rh, Ir) are compared. This allows for a more complete understanding of the relationship between magnetism and superconductivity and of why certain structure types favor heavy-fermion superconductivity.

Experimental Section

Synthesis. La (99.999%) and Ce (99.999%) metals obtained from Ames Laboratory, and In ingot (Alfa Aesar, 99.9995%), were cut into small pieces. Rh (Alfa Aesar, −20 mesh, 99.95%) and Ir (Alfa Aesar, −60 mesh, 99.95%) powders were used as received.

Ln_2MIn_8 (Ln = La, Ce; M = Rh, Ir) single crystals were grown from excess In flux. Stoichiometric amounts of Ln = La, Ce and M = Rh, Ir were combined with excess In in an alumina crucible, which was then encapsulated in an evacuated quartz ampule. The evacuated quartz ampule was heated at 1100 °C for 2 h and slow-cooled at a rate of 8 °C/h to 650 °C. At this temperature, the ampule was removed from the furnace, and excess In flux was removed by centrifugation.[16]

Single-Crystal X-ray Diffraction. The ∼1 × 2 mm metallic platelike crystals were mechanically separated for structural analysis. All of the crystals were stable in air, and no noticeable degradation of the sample was observed in magnetic measurements.

A black single-crystal fragment of each compound was used for data collection on a Nonius KappaCCD diffractometer (Mo K_α, $\lambda = 0.71073$ Å). Data were collected at 298 K. Further data collection parameters and crystallographic data are presented in Table 1.

The structures were solved with direct methods and refined using SHELXL97[17] beginning with the atomic positions of Ho_2CoGa_8 as the initial structural model.[18] Data were corrected for extinction and refined with anisotropic displacement parameters. The atomic coordinates are provided in Table 2, and relevant interatomic distances are given in Table 3.

Largest features in the final difference maps are 8.18 $e^-/Å^3$ for Ce_2RhIn_8, 6.6 $e^-/Å^3$ for Ce_2IrIn_8, 15.9 $e^-/Å^3$ for La_2RhIn_8, and 31.8 $e^-/Å^3$ for La_2IrIn_8. Low-temperature (100 K) data were also collected, and the large features existed in these difference maps. These residual electron densities are higher than expected, even for lanthanide-containing compounds. When a light atom, such as O, is placed in that position, the refinement gives a slightly less than fully occupied site (∼97% for La_2RhIn_8), and the *R*-value changes very little. Furthermore, the electron-density peaks are at ($^1/_2$, $^1/_2$, 0), a 4/*mmm* site approximately octahedrally surrounded by In atoms. In Ce_2RhIn_8, five of the In atoms were located 2.35 Å from this electron density, and the sixth In was 2.42 Å away. This hole is too small for a heavy element, such as In, to occupy the site. The electron density may suggest an interstitial presence of a small-*Z* atom; therefore, we also conducted microprobe analysis to address the possible presence of C, N, or O.

Electron Microprobe Analysis. To determine the presence of an interstitial atom, we examined a single crystal of each compound: Ce_2RhIn_8, Ce_2IrIn_8, La_2RhIn_8, and La_2IrIn_8. Analyses were performed on a JEOL733 Superprobe at 15 kV accelerating potential and 10 nA beam current. WDS scans were made on diamond and BN standards at 1.0 s/point in 5-μm intervals. After locating the C and N peak positions, we found no evidence for the presence of C, N, or O. Because other evidence of the presence of a light atom cannot be found, and given the crystal quality of the sample, we suspect that the residual electron densities may be due to systematic error. A number of crystal growth attempts yielded similar crystal quality.

Physical Properties. Electrical resistivity and magnetic susceptibility data were obtained using commercial measurement systems from Quantum Design (PPMS and MPMS, respectively). Data were collected over a temperature range of 2 K to 350 K.

Results and Discussion

The structures of $LnMIn_5$ ($n = 1$; Ln = La, Ce; M = Co, Rh, Ir) have been previously described in detail.[19−21] The structure consists of one $LnIn_3$ cuboctahedra layer interleaved with one MIn_2 layer. As the transition metal progressively increased in size, the height of the cuboctahedra along the *c*-axis decreased while the length across the *a*−*b* plane increased. Interestingly, the $LnIn_3$ (Ln = La, Ce) cuboctahedra in $LnMIn_5$ were distorted for the M = Co, Ir members, but were least distorted for M = Rh. The cuboctahedra in $LnRhIn_5$ (Ln = La, Ce) bear a striking resemblance to the cubic structure of $LnIn_3$ but are distorted for $LnCoIn_5$ and $LnIrIn_5$.[21] Thus, one might speculate that the reason that $CeRhIn_5$ orders magnetically ($T_N = 3.8$ K) while $CeIrIn_5$ and $CeCoIn_5$ superconduct (at 0.4 and 2.3 K, respectively) is related to this distortion.

Ln_2MIn_8 (Ln = La, Ce; M = Rh, Ir) crystallize in the tetragonal space group, *P*4/*mmm* (no. 123) with the Ho_2CoGa_8 structure type.[18] The structure can be viewed as a *bi*layer of $LnIn_3$ cuboctahedra layers alternating with MIn_2 rectangular polyhedra layers along the *c*-axis. The unit cell is shown in Figure 1, and the extended structures of the Ln_nRhIn_{3n+2} family ($n = 1, 2, \infty$; Ln = La, Ce) are compared in Figure 2. Atomic positions of Ln_2MIn_8 (Ln = La, Ce; M = Co, Rh, Ir) are presented

(9) Buschow, K. H. J.; de Wijn, H. W.; van Diepen, A. M. *J. Chem. Phys.* **1969**, *50*, 137.
(10) Thompson, J. D.; Movshovich, R.; Fisk, Z.; Bouquet, F.; Curro, N. J.; Fisher, R. A.; Hammel, P. C.; Hegger, H.; Hundley, M. F.; Jaime, M.; Pagliuso, P. G.; Petrovic, C.; Phillips, N. E.; Sarrao, J. L. *J. Magn. Magn. Mater.* **2001**, *226−230*, 5.
(11) Mathur, N. D.; Grosche, F. M.; Julian, S. R.; Walker, I. R.; Freye, D. M.; Haselwimmer, K. W.; Lonzarich, G. G. *Nature* **1998**, *394*, 39.
(12) Knebel, G.; Braithewaite, D.; Canfield, P. C.; Lapertot, G.; Flouquet, J. *Phys. Rev. B* **2001**, *65*, 02445.
(13) Satoh, K.; Fujimaki, Y.; Umehara, I.; Itoh, J.; Onuki, Y.; Kasaya, M. *Physica B* **1993**, *186−188*, 658.
(14) Benoit, A.; Boucherle, J. X.; Convert, P.; Flouquet, J.; Palleau, J.; Schweizer, J. *Solid State Commun.* **1980**, *34*, 293.
(15) Berton, A.; Chaussy, J.; Chouteau, G.; Cornut, B.; Flouquet, J.; Odin, J.; Palleau, J.; Peyard, J.; Tournier, R. *J. Phys.* **1979**, *40*, 325.
(16) Canfield, P. C.; Fisk, Z. *Philos. Mag. B* **1992**, *65*, 1117.
(17) Sheldrick, G. M. *SHELXL97*; University of Gottingen: Germany, 1997.
(18) Grin, Y. N.; Yarmolyuk, Y. P.; Gladychevskii, E. I. *Sov. Phys. Crystallogr.* **1979**, *24*, 137.
(19) Moshopoulou, E. G.; Fisk, Z.; Sarrao, J. L.; Thompson, J. D. *J. Solid State Chem.* **2001**, *158*, 25.
(20) Moshopoulou, E. G.; Sarrao, J. L.; Pagliuso, P. G.; Moreno, N. O.; Thompson, J. D.; Fisk, Z.; Ibberson, R. M. *Appl. Phys. A, Mater. Sci. Proc.* **2002**, *74*, S-895−S-897.
(21) Macaluso, R. T.; Sarrao, J. L.; Pagliuso, P. G.; Moreno, N. O.; Goodrich, R. G.; Browne, D. A.; Fronczek, F. R.; Chan, J. Y. *J. Solid State Chem.* **2002**, *166*, 245.

Table 1. Crystallographic Parameters for Ce_2RhIn_8, Ce_2IrIn_8, La_2RhIn_8, and La_2IrIn_8

Crystal Data		
formula	**Ce_2RhIn_8**	**Ce_2IrIn_8**
a (Å)	4.6670(4)	4.6897(6)
c (Å)	12.247(4)	12.1950(11)
V (Å^3)	266.75(12)	266.07(5)
Z	1	1
temperature (°C)	25	25
density (g cm^{-3})	8.013	8.681
crystal dimension (mm^3)	0.075 × 0.025 × 0.075	0.075 × 0.050 × 0.025
crystal system	tetragonal	tetragonal
space group	*P*4/*mmm*	*P*4/*mmm*
θ range (°)	2.5−45.3	2.5−35.0
μ (mm^{-1})	26.703	37.711
Data Collection		
measured reflections	1129	1204
independent reflections	703	408
reflections with $I > 2\sigma(I)$	606	372
R_{int}	0.032	0.068
h	-9 → 9	-7 → 7
k	-6 → 6	-7 → 7
l	-23 → 24	-19 → 19
Refinement		
$R [F^2 > 2\sigma (F^2)]$	0.042	0.047
$wR(F^2)$	0.1012	0.108
reflections	703	408
parameters	17	17
$\Delta\rho_{max}$ (e Å^{-3})	8.12	6.6
$\Delta\rho_{min}$ (e Å^{-3})	-2.9	-2.9
extinction coefficient	0.0073(8)	none
Crystal Data		
formula	**La_2RhIn_8**	**La_2IrIn_8**
a (Å)	4.6980(2)	4.70600(10)
c (Å)	12.3440(4)	12.3120(4)
V (Å^3)	272.447(19)	272.667(12)
Z	1	1
crystal dimension (mm^3)	0.075 × 0.012 × 0.075	0.10 × 0.050 × 0.075
temperature (°C)	25	25
density (g cm^{-3})	7.919	8.456
crystal system	tetragonal	tetragonal
space group	*P*4/*mmm*	*P*4/*mmm*
θ range (°)	3.3−45.3	2.5−40.2
μ (mm^{-1})	25.63	36.29
Data Collection		
measured reflections	2197	1697
independent reflections	730	579
reflections with $I > 2\sigma(I)$	592	570
R_{int}	0.065	0.054
h	-9 → 9	-8 → 8
k	-6 → 6	-6 → 6
l	-22 → 24	-22 → 20
Refinement		
$R [F^2 > 2\sigma (F^2)]$	0.059	0.054
$wR(F^2)$	0.151	0.142
reflections	730	579
parameters	17	17
$\Delta\rho_{max}$ (e Å^{-3})	15.9	31.8
$\Delta\rho_{min}$ (e Å^{-3})	-4.1	-7.6
extinction coefficient	0.015(2)	0.016(2)

[a] $R_1 = \sum||F_o| - |F_c||/\sum|F_o|$. [b] $wR_2 = \sum[w(F_o^2 - F_c^2)]/\sum[w(F_o^2)^2]^{1/2}$.

in Table 2. The *z* coordinates of the 2*g*, 4*i*, and 2*h* sites are variable for Ce, In2, and In3, where In2 and In3 correspond to the In atoms that are bonded to the MIn_2 and $LnIn_3$ layers, respectively.

The bond distances describing the cuboctahedra in Ln_2MIn_8 (Ln = La, Ce; M = Rh, Ir) are listed in Table 4. Ce is located at the center of each cuboctahedron. Ce and In3 are across the a−b plane, but the two atoms are not strictly coplanar as in $LnMIn_5$. (Ce−In1) is the bond between the Ce and the In atom (In1) between the two $CeIn_3$ layers. (Ce−In2) describes the bond between Ce and the In atom (In2) that is shared with the MIn_2 (M = Rh, Ir) layer.

Selected interatomic distances of the cuboctahedra layer in Ln_2MIn_8 compounds are shown in Table 3. The width of the cuboctahedra along the *a*−*b* plane (Ln−In3) and part of the cuboctahedra height along the *c*-axis (Ln−In2 distance) are smaller for the Ir than the Rh compound. In the $LnMIn_5$ phase however, the cuboctahedra width is larger for Ir. However, Ln_2MIn_8 contains a third crystallographically independent In atom whose distance to the next cuboctahedra layer (Ln−In1) in-

Table 2. Atomic Positions of Ln_2MIn_8 (Ln = La, Ce)

atom		*x*	*y*	*z*
Ln	2*g*	0	0	*z* Ln
Rh	1*b*	0	0	1/2
In1	2*f*	1/2	0	0
In2	4*i*	1/2	0	*z*In2
In3	2*h*	1/2	1/2	*z*In3

compound	*z* Ln	*z* In2	*z* In3
Ce_2RhIn_8	0.80704(3)	0.61944(4)	0.80563(6)
Ce_2IrIn_8	0.80602(8)	0.61993(9)	0.80562(11)
La_2RhIn_8	0.80631(5)	0.61788(5)	0.80364(9)
La_2IrIn_8	0.80527(5)	0.61833(5)	0.80368(9)

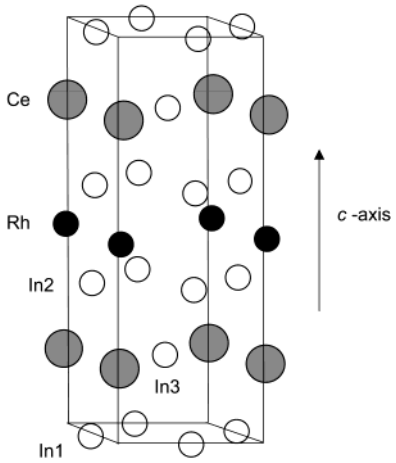

Figure 1. Unit cell of Ce_2RhIn_8. Gray, black, and white circles represent Ce, Rh, and In atoms, respectively.

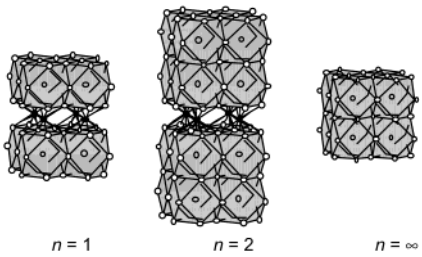

Figure 2. Structures of the $n = 1, 2, \infty$ members of the Ce_nRhIn_{3n+2} family. White circles represent In, black circles represent Rh, and gray shading represents Ce cuboctahedra.

creases. This compensates for the decrease in (Ln−In2) and avoids extreme cuboctahedra distortions.

The ratios of (Ce−In3/Ce−In1) and (Ce−In3/Ce−In2) describe the degree of structural distortion in the cuboctahedra of Ce_2MIn_8. For both M = Rh and Ir, (Ce−In3/Ce−In1) have identical deviations (0.0064) from unity, as shown in Table 4. The (Ce−In3/Ce−In2) ratio is closer to 1 in the Rh compound than in the Ir compound, indicating that the cuboctahedra in Ce_2RhIn_8 resembles the cubic structure of $CeIn_3$ more so than Ce_2IrIn_8. Thus, Ce_2RhIn_8 is more 3D and more like $CeIn_3$ than Ce_2IrIn_8. Similar to $CeRhIn_5$, the less distorted local geometry in Ce_2RhIn_8 may be related to why it orders magnetically whereas Ce_2IrIn_8 does not. The La−In distances are slightly larger in the Ce analogues, as expected, due to lanthanide contraction. Similar trends in the (La−In3/La−In1) and (La−In3/La−In2) ratios are found for the La analogues. This trend has also been observed for the $LnMIn_5$ (Ln = La, Ce; M = Rh, Ir) subfamily.[21]

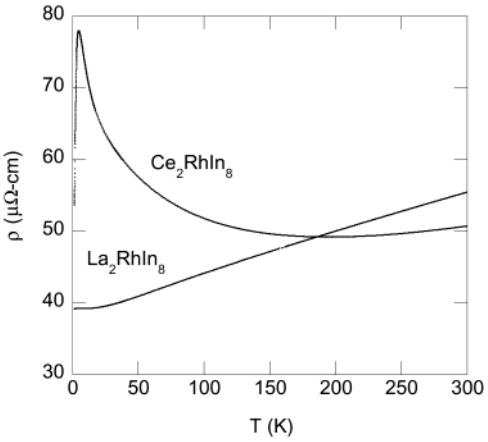

Figure 3. Electrical resistivity (ρ_o) as a function of temperature (*T*) for Ce_2RhIn_8 and La_2RhIn_8.

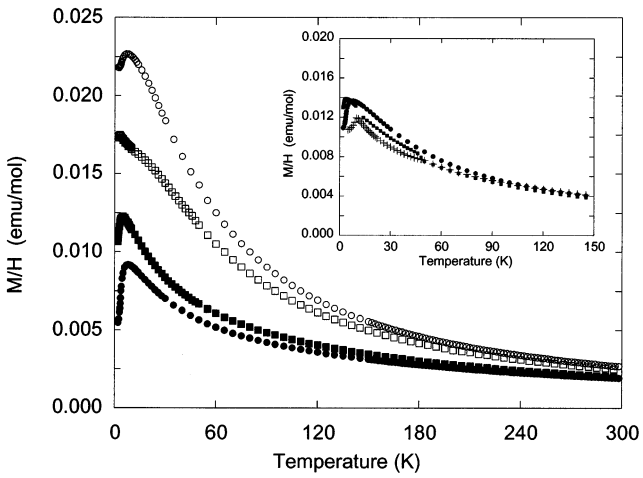

Figure 4. Magnetic susceptibility *M*/*H* as a function of *T*, measured at 1000 Oe. Circles represent $CeRhIn_5$, squares represent Ce_2RhIn_8, and crosses represent $CeIn_3$. Open symbols are for applied field parallel to the crystallographic *c*-axis and solid symbols are for H perpendicular to *c*. The inset shows the polycrystalline average of these data ($^1/_3[\chi_{parallel} + 2\chi_{perpendicular}]$) in comparison to those of cubic $CeIn_3$.

Relation of Structural Parameters to Physical Properties. *Resistivity.* The temperature dependence of the electrical resistivity of the Ln_2MIn_8 family is qualitatively similar to that of $LnMIn_5$. In particular, for the La variants, the resistivity is that of a normal metal, whereas for the Ce variants one observes resistivity that is relatively temperature independent above a characteristic temperature $T \sim 20$ K before becoming more metallic.[3] Representative data for Ln_2RhIn_8 are shown in Figure 3.

Strikingly, the residual resistivity (ρ_o) of Ce_2RhIn_8 ($\rho_o = 55$ $\mu\Omega$-cm) is 2 orders of magnitude larger than that of $CeRhIn_5$ ($\rho_o = 0.4$ $\mu\Omega$-cm); similar differences are observed in the La analogues. This effect is much more significant than any observed variations as a function of homologous series in a particular structure type. We speculate that this increased resistivity results from the buckling of the Ln−In3 layer. The In3−Ln−In3 bond angles are provided in Table 3. In Ce_2RhIn_8, Ce and In3 no longer reside in the same a−b plane, and the In3−Ce−In3 angle is no longer 180° as in the $CeRhIn_5$. The *z*Ce coordinate is 0.80704(3) while *z*In3 is 0.80563(6), resulting in the formation a 179.40(2)° In3−Ce−In3

Table 3. Select Interatomic Distances (Å) and Bond Angles for Ln_nMIn_{3n+2} (n = 2; Ln = La, Ce; M = Rh, Ir)

	Ce_2RhIn_8	Ce_2IrIn_8	La_2RhIn_8	La_2IrIn_8
Within $LnIn_3$ (Ln = La, Ce) Cuboctahedron				
Ce(La)−In1 (× 4) (Å)	3.3001(5)	3.3242(7)	3.3520(5)	3.3593(5)
Ce(La)−In2 (× 4) (Å)	3.2748(4)	3.2565(10)	3.3060(6)	3.2915(6)
Ce(La)−In3 (× 4) (Å)	3.3211(3)	3.3029(4)	3.32215(14)	3.3277(5)
In3−Ce(La)−In3 Angle (°)	179.40(2)	179.83(5)	178.86(4)	179.32(4)
Within MIn_2 (M = Rh, Ir) Rectangular Polyhedron				
In2−In2 (*c*-axis)	2.9255(9)	2.925(2)	2.9107(13)	2.9138(13)
In1−In1 (*a*-*b* plane)	3.3001(5)	3.3029(4)	3.32199(14)	3.3276(5)
M−In2 (× 8) (Å)	2.7541(3)	2.7556(6)	2.7633(4)	2.7675(3)

Table 4. Ln−Ln Bond Distances in $LnIn_3$ (Ln = La, Ce) Cuboctahedra

	Ce−In1 (Å)	Ce−In2 (Å)	Ce−In3(Å)	Ce−In3/Ce−In1(Å)	Ce−In3/Ce−In2(Å)
Rh	3.3001(5)	3.2748(4)	3.3211(3)	1.0064(2)	0.9981(1)
Ir	3.3242(7)	3.2565(10)	3.3029(4)	0.9936(2)	1.0142(3)
	La−In1 (Å)	La−In2 (Å)	La−In3(Å)	La−In3/La−In1(Å)	La−In3/La−In2(Å)
Rh	3.3520(5)	3.3060(6)	3.32215(14)	0.9911(1)	1.0049(2)
Ir	3.3593(5)	3.2915(6)	3.3277(5)	0.9906(2)	1.0110(2)

angle. Buckling of the Ln atom is increased in the nonmagnetic La-analogues. For example, the In3−La−In3 angle measures 178.86(4)° in La_2RhIn_8, almost 1° smaller than its Ce analogue.

Magnetic Susceptibility. The magnetic susceptibility as a function of temperature for Ce_nRhIn_{3n+2} (n = 1, 2, ∞) is shown in Figure 4. In each case, the susceptibility is approximately what is expected from a Ce J = 5/2 local moment, namely Curie−Weiss susceptibility at high temperature with μ_{eff} close to 2.54 μ_B ($\mu_{eff} = (8C)^{1/2}$ and $\chi = \chi_o + C/(T + \theta)$). Specifically, for field applied perpendicular to the crystallographic *c*-axis, χ_o = −0.00019(1) emu/mol, C = 0.807(5) (μ_{eff} = 2.534(5) μ_B), and θ = −70.7(8) K; for field parallel to the *c*-axis, χ_o = −0.00035(2) emu/mol, C = 0.899(7) (μ_{eff} = 2.674(7) μ_B), and θ = −18.2(8) K.

For the tetragonal compounds, magnetic anisotropy is observed, and this anisotropy is larger in single-layer $CeRhIn_5$ than in Ce_2RhIn_8. Interestingly, if one performs a polycrystalline average of the data ($\chi_{poly} = {}^1/_3 (2\chi_a + \chi_c)$), the data for all three compounds are nearly identical. This indicates that although structural layering modifies the magnetic character of these compounds, the overall effect is rather small. The evolution of the magnetic ordering temperature, on the other hand, is something of a mystery: naively, one would expect T_N to evolve in the order of $CeIn_3$, Ce_2RhIn_8, $CeRhIn_5$, consistent with decreasing 3-D character. However, one finds T_N ($CeRhIn_5$) > T_N (Ce_2RhIn_8). This is presumably due to differences in the electronic structure of these materials, which are also reflected in the propagation vectors of the ordered magnets. $CeIn_3$ and Ce_2RhIn_8 have nearly the same magnetic structure, whereas the structure of $CeRhIn_5$ is more helical and 2-D.[7] The low-temperature heavy-fermion ground states of $CeMIn_5$ and Ce_2MIn_8 (M = Rh, Ir) have been studied using specific heat measurements and are least affected by the structural layering. The γ values are 400 mJ/mol Ce K^2 for both $CeRhIn_5$ and Ce_2RhIn_8, and 720 mJ/mol Ce K^2 and 700 mJ/mol Ce K^2 for $CeIrIn_5$ and Ce_2IrIn_8, respectively.[2] These observations are consistent with the fact that hybridization is a relatively local effect; the local Ce coordination is not changed between the n = 1 and n = 2 members of the Ce_nMIn_{3n+2}family.

Conclusion

The structure, magnetic, and transport properties clearly show that the Ce_nMIn_{3n+2} family (n = 1, 2, ∞; M = Rh, Ir) becomes more three-dimensional as one progresses from $n = 1 \rightarrow \infty$. The key structural feature of the Ln_nMIn_{3n+2} family lies within the $LnIn_3$ cuboctahedra. In particular, the half of the cuboctahedra closest to the MIn_2 layer is most significant. Ratios of Ce−In and Ce−Ce distances explain the dimensionality and anisotropy observed in magnetic susceptibility measurements. This is consistent with magnetic structure studies of Ce_nRhIn_{3n+2} where the cubic $CeIn_3$ building blocks have a stronger influence on magnetic correlation than $RhIn_2$.[7] In addition, the Ce buckling within the cuboctahedra contributes to increased resistivity for both the Ce-based and La-based materials.

Acknowledgment. R.T.M. acknowledges Dr. Xiaogang Xie for his help with the SEM/Microprobe analysis. Work at LANL was performed under the auspices of the U.S. Department of Energy. J.Y.C. acknowledges the Louisiana Board of Regents, PRF-G, and NSF for partial support of this project.

Supporting Information Available: Crystallographic data in CIF format are available for Ce_2RhIn_8, Ce_2IrIn_8, La_2RhIn_8, and La_2IrIn_8. This material is available free of charge via the Internet at http://pubs.acs.org.

CM021063E